

# Optimization on Thermal Management of Lithium-Ion Batteries Using Computational Fluid Dynamics and Air-cooling Methods

Hong Shi<sup>1,\*</sup>, Meinan Liu<sup>1</sup>, Wenbing Xu<sup>1</sup>, Xinlong Zhu<sup>2</sup>, Yitao Zou<sup>2</sup>, Kaijie Yang<sup>2</sup>

<sup>1</sup> College of Energy & Power Engineering, Jiangsu University of Science and Technology, 2 Mengxi, Jingkou, Zhenjiang 212003, China

<sup>2</sup> Key Laboratory of Aircraft environment control and life support, MIIT, Nanjing University of Aeronautics & Astronautics, 29 Yudao Street, Nanjing 210016, China

\*E-mail: [shihong@nuaa.edu.cn](mailto:shihong@nuaa.edu.cn)

Received: 9 February 2022 / Accepted: 12 March 2022 / Published: 5 April 2022

---

Lithium-ion batteries are key components in cargo container-type large capacity energy system. It is essential to maintain temperature and thermal profile of the battery pack within the desired range in order to ensure its cycle life. Based on computational fluid dynamics (CFD) method, a periodic air-cooling method is proposed to improve the temperature distribution of the batteries. The effects of 3 different air-cooling method on heat dissipation and energy saving of the battery pack are compared. The results indicated that: (1) The directional air supply method can significantly restrain temperature rise of the batteries in the middle of the battery pack, but it is hard to blow to the side, which easily lead to uneven temperature distribution. (2) By changing the air supply direction, the periodic airflow can enhance the airflow disturbance, improve the heat dissipation effect and thermal uniformity of the battery. (3) With the directional airflow method, reducing the airflow temperature and increasing the airflow rate can nearly achieve the same result as periodic air-cooling method, but the latter is more energy efficient. This paper provided a new approach to the battery thermal management under energy saving conditions.

---

**Keywords:** Container, Battery Thermal Management, Periodic Airflow, Energy Saving, CFD

## 1. INTRODUCTION

The cargo container-type large capacity energy system with closely arranged lithium-ion rechargeable batteries as a new storing energy device with obvious advantages such as high reliability and strong environmental adaptability, attracting more and more attention [1]. Especially, its characteristics are closely related to the performance of the batteries [2-3]. Batteries is awfully sensitive to temperature owing to its chemistry [4-6], excessive temperature or thermal non-uniformity would reduce the cycle life of battery pack [7-8]. Therefore, to meet the battery requirements of efficiency and safety, the optimal temperature should be controlled in an operating range of 288~313 K [9-10], the

temperature difference between individual batteries should not exceed 5 K [11]. Therefore, the cooling system plays an important role in cargo container-type large capacity energy system to ensure the battery security.

Many advanced cooling methods can be used [12-14]: the liquid cooling, the air-cooling, the heat pipe cooling and the phase change material cooling. However, the air-cooling method dominates due to the operating cost, potential safety, and layout limitation. As the optimum selection of battery thermal management, air-cooling consists of nature cooling and forced cooling [15-16]. The latter has simple structure and low cost, which has important engineering significance [17]. Considering the wide application of computational fluid dynamics (CFD) method in heat transfer enhancement, researchers had carried out systematically many investigations on the heat dissipation of the battery pack by forced air cooling through CFD methods.

The temperature distribution of the batteries is significantly influenced by thermal boundary conditions, which has been proven by many researchers. Zhang et al. [18] analysis that forced thermal convection conditions led to relatively small temperature increase but comparatively large temperature gradient. However, Li et al. [19] found that the increase of heat transmission coefficient restricting the temperature rise in the battery pack. Panchal et al. [20-21] pointed out that increasing discharge rates and operating temperature would increase the heat fluxes at battery by experimental and theoretical method. Mahamud et al. [22] demonstrated the reciprocating airflow for cooling would improve temperature uniformity and decrease the maximum temperature of the battery.

But in fact, enhanced heat transfer has limitations in improving temperature uniformity. For instance, active heat transfer enhancement means that more energy will be consumed. Thus, as a passive thermal optimization technology, cooling configuration design has been widely concerned and recognized [23]. Wang et al. [24] carried out the numerical simulation of a cargo container-type large capacity energy system, optimized by adding a wind guide plate in the air channel. Similarly, Yang et al. [25] investigated the effect of size and layout angle of the guide plate on the air flow and heat transfer characteristics. Fan et al. [26] pointed out that reducing the channel widths or increasing the airflow rate is beneficial to decreasing the battery temperature. Besides, Shi et al. [27] investigated the influences of four factors (setting a new air inlet, air inlet position, air inlet size, and gap size between the cells and the back wall) on the battery pack and the optimized battery pack structure was obtained.

In summary, the previous studies focus more on changing the model structure to optimize the heat dissipation effect. However, cargo container-type large capacity energy system generally uses normalized batteries, which limits the space for thermal design optimization of batteries. Also, the gaps among battery cells are only a few millimeters, which especially limits the structural changes. Therefore, the above results are not suitable for solving the problem of intensive heat dissipation of the container energy storage batteries.

In this paper, the temperature distributions of the battery pack are investigated by CFD methods, and a new air-cooling method with the periodic airflow is proposed. On this basis, the influence of the periodic airflow on heat dissipation and energy saving is analyzed. The results provide reference for thermal management of cargo container-type large capacity energy system.

## 2. THEORY AND MATHEMATICAL MODELING

The battery pack consists of 24 polymer lithium iron phosphate powered batteries and 4 coolant passages, which are divided into 3 groups, the No.1-No.8 battery cells are defined as the first group, the No.9-No.16 battery cells are defined as the second group, and the No.17-No.24 battery cells are defined as the third group. The size of the battery pack is 698 mm × 515 mm × 188 mm (length × width × height) as shown in Figure 1(a). The gap between each battery group is 35 mm, and the gap *d* between battery cells in each group is 15 mm. The size of a battery cell is 174 mm × 47 mm × 127 mm (length × width × height). The battery pack model is shown in Figure 1(b). The area and height of the inlet and the outlet are shown in Figure 1(c) and Figure 1(d) separately.

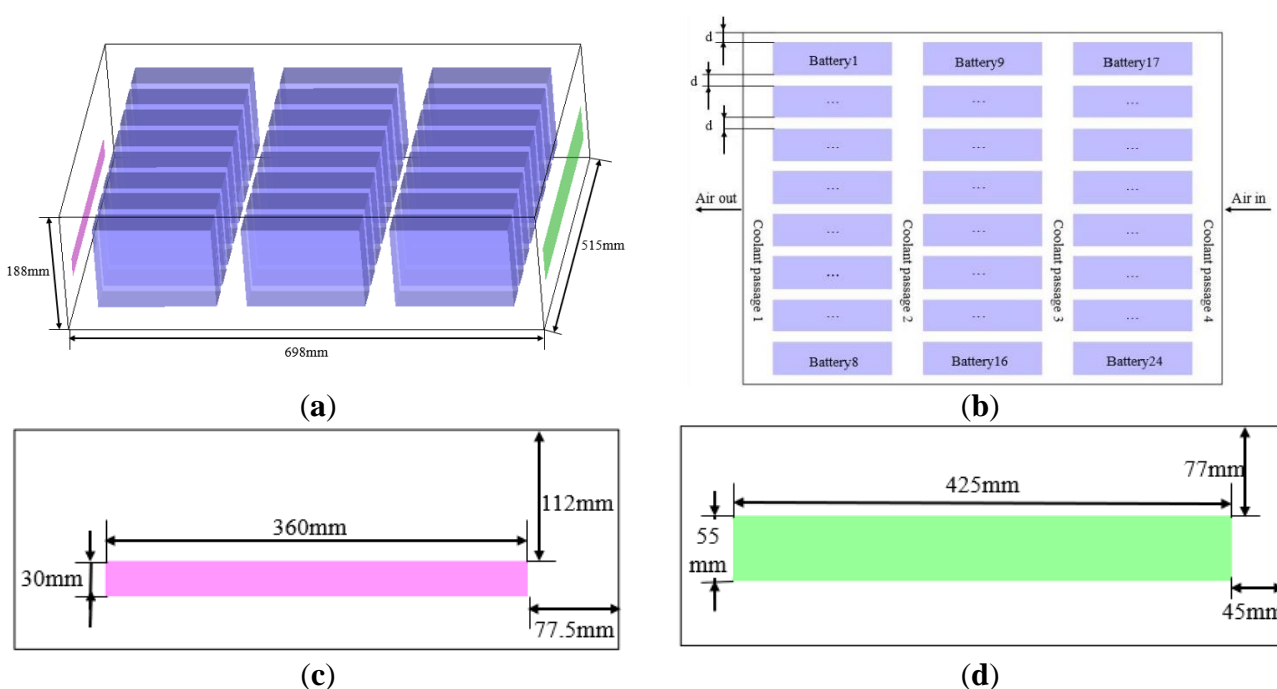


**Figure 1.** Model of the battery pack: (a) Schematic diagram of the battery pack; (b) Top view of the battery pack; (c) Left view of the battery pack; (d) Right view of the battery pack.

**Table 1.** Specification parameter table of lithium iron phosphate battery

Parameter	Value
Nominal capacity/Ah	60
Nominal voltage/V	3.2
Internal resistance/mΩ	≤1.0
Maximum charge/discharge C rate	1/2
Size/mm	174 × 47 × 127
Weight/kg	1.55 ± 0.03

In order to estimate the heat generation rate, the theoretical calculation model proposed by Bernardi was used [28]:

$$q_v = \frac{I}{V_b} \left[ (U_o - U) + T \frac{\partial U_o}{\partial T} \right] = \frac{1}{V_b} \left( I^2 R_b + IT \frac{\partial U_o}{\partial T} \right) \quad (1)$$

Where  $q_v$ (W) means the heat generation rate per unit volume,  $V_b$  ( $m^3$ ) means battery volume.  $U_o$  (V),  $U$  (V) and  $I$  (A) means open-circuit voltage, working voltage and cell current, respectively.  $T$  (K) means absolute temperature.  $R_b$  ( $\Omega$ ) means battery internal resistance. According to equation (1),  $q_v$ (W) of the battery cells in this paper is calculated to be  $4022.33 \text{ W/m}^3$ .

### 3. NUMERICAL SIMULATION

#### 3.1 Boundary conditions

Although the battery is a volume heat source, it is simplified to a surface heat source in order to decrease the number of grids and reduce the computational time. Boundary conditions are set as realistic as possible [29]. The inlet boundary condition is air flow velocity at 2 m/s. The outlet boundary condition is pressure-outlet. The temperature around the battery pack is 300 K, which is the same as the airflow temperature. ANSYS-Fluent 18.0 was utilized in this paper. The total solution time is 6.5 s, and time step increment is  $10^{-4}$  s, calculated with transient method. The calculation is convergence when all the residuals are less than  $10^{-5}$ .

#### 3.2 Meshing validation

The structured element meshing is built by ANSYS ICEM. To improve the accuracy, the boundary layer encryption processing is performed. 4 cases are simulated in the grid independence analysis, the maximum temperature of the battery at 3 s is selected as the metric, as shown in Table 2.

**Table 2.** Grid independence verification

case	Number of grids (million)	The highest temperature of the cooling surface at 3 s (K)
1	1.90	304.6
2	3.05	305.2
3	4.76	307.1
4	5.88	307.2

It can be seen from the results that the appropriate number of grids is  $4.76 \times 10^6$ , since the metrizable shows not obviously ameliorates when the number of grids continuously increased.

### 3.3 Algorithm verification

To verify the simulation method, a model used in this paper is the same as that in the literature [30], as is shown in Figure 2(a). Figure 2(b) shows the comparison between the predicted numerical results and the experimental data obtained by Xie’s study. In particular, an analysis is performed to compare the accuracy of different eddy-viscosity turbulence models for simulations of BTMS.

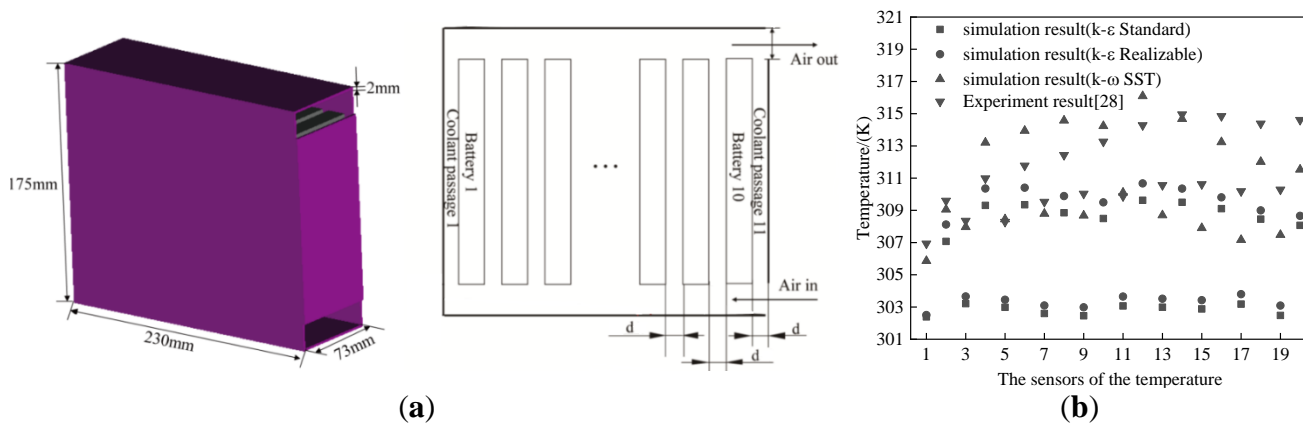


**Figure 2.** Algorithm verification: (a) Schematic diagram of the algorithm verification model; (b) Comparison of monitoring points under experimental [28] and simulated conditions.

From Figure 2(b), it can be concluded that the k- $\omega$  SST model is to be preferred over the other models, because the numerical simulation results of the k- $\omega$  SST model are in better agreement with the experimental results. Therefore, the k- $\omega$  SST model used in the CFD simulation of BTMS proved to have sufficient accuracy to predict the temperature distribution of the battery pack.

## 4. RESULTS AND DISCUSSION

### 4.1 Battery performance index

Three indices are put forward to estimate the thermal performance.  $T_{max}$  (K) is the highest temperature of cells,  $\Delta T$  (K) is the maximum temperature difference among batteries, for simplicity, the temperature of each battery cell is defined as the average temperature,  $\sigma$  is the standard deviation of the temperature value of 5000 random points of cells. A smaller value of  $T_{max}$  means better cooling effect, and a smaller value of  $\Delta T$  and  $\sigma$  means better uniformity of temperature distribution. The three indices are obtained by numerical simulations.

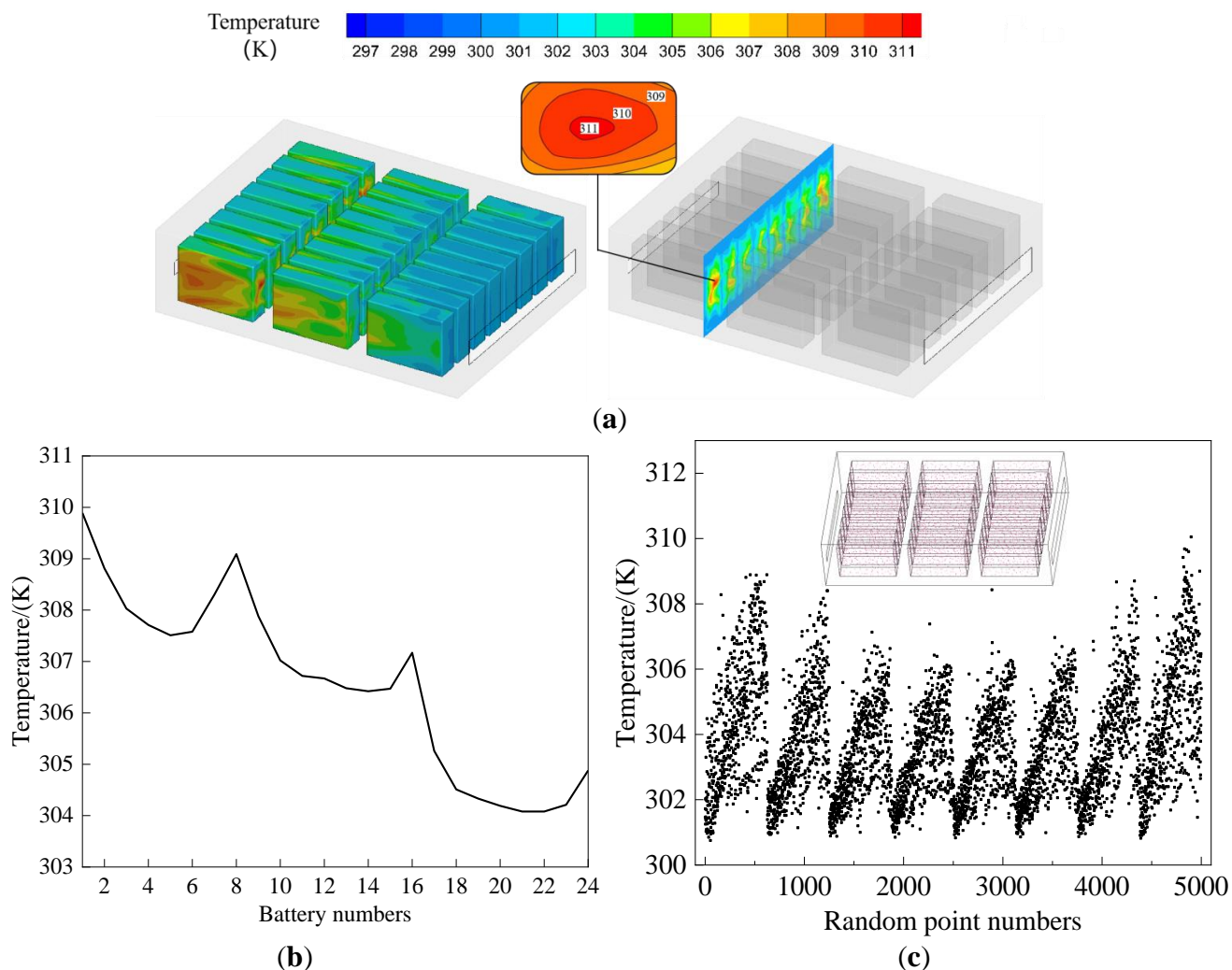


**Figure 3.** Simulation results of Case I: (a) Temperature distribution of batteries; (b) Temperature of the single battery; (c) Temperature of 5000 random points.

It is found from Figure 3(a) that  $T_{max}$  is 311 K, and one of the highest temperature regions is located on the right side of No.8 battery, predicted for this basic case. As presented in Figure 3(b), No.1 battery has the highest average temperature of 309.9 K, while No.21 battery has the lowest average temperature of 304.1 K,  $\Delta T$  is 5.8 K, and the battery temperature in mid-position of each group is clearly lower than that on both sides. In addition, the downstream temperature of batteries is always higher than the upstream temperature along the airflow direction. The average surface temperature values of each battery are relatively different, mainly because the interval between adjacent batteries is inadequately large. As can be seen from Figure 3 (c), 5000 random points are randomly selected,  $\sigma$  is 2.87.

In the case of directional air supply, although Case I has the advantage of achieving a lower  $T_{max}$ , it has a disadvantage of non-uniformity temperature distribution, that the maximum temperature difference  $\Delta T$  exceeding the range of specified operating temperature. As a result, conventional optimization methods aren't adopted to meeting the requirements of the battery thermal management.

#### 4.2 Simulation results of conventional optimization methods

The temperature distribution of Case I is presented in Figure 3(a) and Figure 3(b). Additionally, Figure 3(c) shows the location of 5000 random points on the battery and the temperature of each point. It is important to note that Case I is served as the basic mode.

##### 4.2.1 Simulation results of increasing air supply speed

In order to improve the thermal environment of batteries, Case II is modified from Case I by increasing the air supply speed, which is varied from 2 m/s to 2.5 m/s. The temperature distribution of Case II is presented in Figure 4(a) and Figure 4(b).

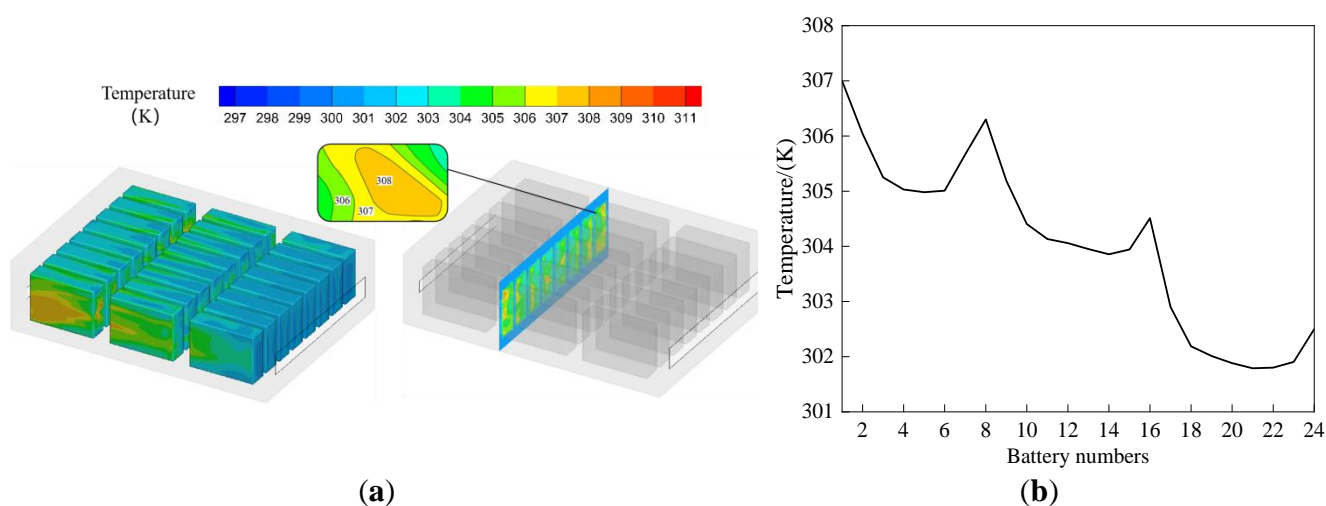


**Figure 4.** Simulation results of Case II: (a) Temperature distribution of batteries; (b) Temperature of the single battery.

It is found from Figure 4(a) that  $T_{max}$  is 308 K, and one of the highest temperature regions is located on the left side of the No.9 battery, predicted for Case II. As presented in Figure 4 (b), No.1 battery has the highest average temperature of 307.0 K, while No.21 battery has the lowest average temperature of 301.8 K,  $\Delta T$  is 5.2 K. Simultaneously, considered of both Figure 4(a) and Figure 4(b), the temperature distribution in Case II is similar to Case I. Additionally,  $\sigma$  is 2.49. Compared with Case I, the maximum temperature of the battery in case II decreased due to the increase of the inlet velocity. It can be seen that growing mass flow rate can significantly decrease the average surface temperature of the battery cells, but the thermal uniformity has no significant improvement.

##### 4.2.2 Simulation results of reducing airflow temperature

In order to improve the thermal environment of batteries, Case III is modified from Case I by decreasing the airflow temperature, which is varied from 300 K to 297 K. The temperature distribution of Case III is presented in Figure 5(a) and Figure 5(b).

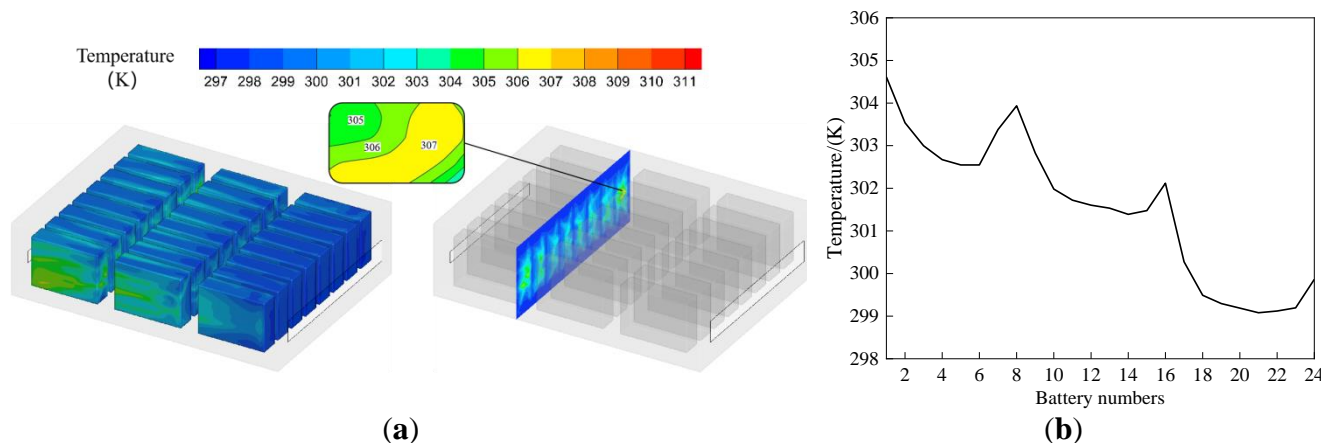


**Figure 5.** Simulation results of Case III: (a) Temperature distribution of batteries; (b) Temperature of the single battery.

It can be seen from Figure 5(a) that  $T_{max}$  is 307 K, and one of the maximum temperature regions is located on the right side of the No.1 battery, predicted for Case III. As presented in Figure 5(b), No.1 battery has the highest average temperature of 304.6 K, while No.21 battery has the lowest average temperature of 299.1 K,  $\Delta T$  is 5.5 K. Taking consideration of both Figure 5(a) and Figure 5(b), the temperature distribution in Case III is also similar to Case I. Additionally,  $\sigma$  is 2.32. Compared with Case I, the fall of the inlet temperature caused Case III have a lower highest temperature, and note that decreasing the airflow temperature has no significant improvement in thermal uniformity.

Although Case III achieves a lower  $T_{max}$ , one negative effect is the higher overall temperature, which cause energy loss.

For Case II, the mass flow rate is improved based on Case I. For Case III, the air flow temperature is decreased based on Case I.  $\Delta T$  is 5.2 K for Case II while 5.5 K for Case III,  $\sigma$  is 2.49 for Case II while 2.32 for Case III. In other words,  $\Delta T$  (and  $\sigma$ ) of Case II and Case III have no obvious difference from the basic case, indicating that changing the boundary conditions is not effective in improving temperature uniformity.

For Lithium-ion batteries, temperature uniformity is a very serious problem to be solved at low energy premise. Accordingly, in the following analysis, instead of changing the boundary conditions, the air flow direction is changed to achieve the purpose of saving energy and meeting the working requirements.

#### 4.3. Optimization design scheme based on periodic air supply

The distribution of mass flow rate should be homogenization method to improve the thermal uniformity of the battery pack. Enhancing the airflow disturbance could significantly improve the uniformity temperature distribution, which can be realized simply by changing the air flow direction. Based on the above, an optimization scheme was proposed to increase the airflow disturbance with

periodically change in air supply direction in order to improve heat dissipation. Besides, a new motion law is introduced with the velocity changes periodically in the x direction and the scalar value remains unchanged. Meanwhile, the motion equation is given. The change of airflow in a period is described in Figure 6, and the equation of motion is shown in equation (2).

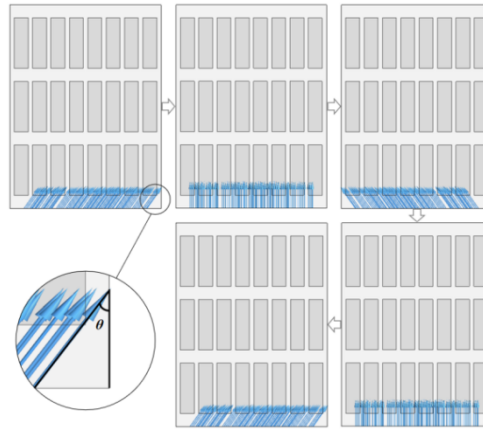


**Figure 6.** Schematic diagram of periodic air supply

$$\begin{aligned}
 V_x &= V_0 \cos(\omega t) \cos \theta \\
 V_y &= \sqrt{V_0^2 - V_x^2}
 \end{aligned}
 \tag{2}$$

Where  $V_x$  (m/s) is the partial velocity in  $x$  direction;  $V_0$  (m/s) represents the airflow velocity in the basic case (Case I);  $\omega$  (rad/s) is the angular velocity of the airflow;  $t$  (s) is the movement time of the airflow;  $\theta$  ( $^\circ$ ) is the angle between the airflow direction and the right side wall of the battery pack at the initial moment;  $V_y$  (m/s) is the partial velocity in  $y$  direction.  $V_0$  can be equal to 2 m/s. It can be seen from Figure 6 that at the initial condition, the air supply direction is specified to be tangent to the No.24 Battery, therefore, the angle  $\theta$  is set to  $31^\circ$  and  $\cos \theta$  is set to 0.829. In this paper,  $\omega$  is set to 1.5. Accordingly,  $V_x$ ,  $V_y$  can be obtained as follows:

$$\begin{aligned}
 V_x &= 0.829 \times 2 \cos(1.5\pi t) \\
 V_y &= \sqrt{2^2 - [0.829 \times 2 \cos(1.5\pi t)]^2}
 \end{aligned}
 \tag{3}$$

To enhance the cooling efficiency and the thermal uniformity, Case IV is modified from Case I by changing the airflow direction, which is changed from directional to periodical. Based on the principles of the periodic airflow movement, the equation (3) was established and applied in UDF. The temperature distribution for Case IV is presented in Figure 7(a) and Figure 7(b). Additionally, Figure 7(c) shows the periodic change of maximum temperature in the battery pack.

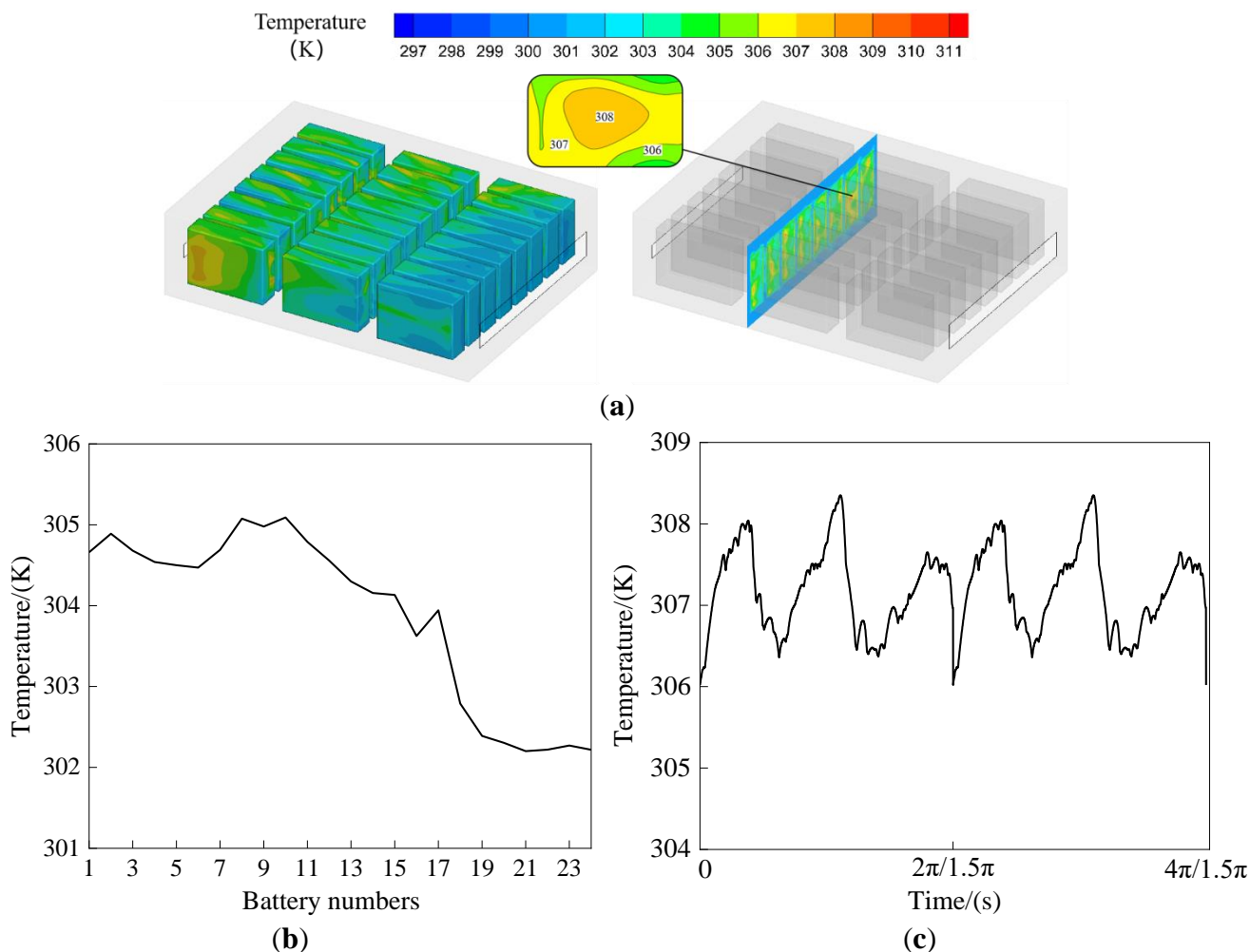


**Figure 7.** Simulation results of Case IV: (a) Temperature distribution of batteries; (b) Temperature of the single battery; (c) Periodic change of maximum temperature.

It can be seen from Figure 7(a) that  $T_{max}$  is 308 K, and one of the highest temperature regions is located on the left side of No.10 battery, predicted for Case IV. As presented in Figure 7(b), No.8 battery has the highest average temperature of 305.1 K, while No.21 battery has the lowest average temperature of 302.3 K,  $\Delta T$  is 2.8 K. Additionally,  $\sigma$  is 1.57. As presented in Figure 7(c), with the periodic variation of the supply air,  $T_{max}$  also presents a periodic variation trend, and is stable after 3.5 s.

As expected, the airflow disturbance affects the temperature distribution. The  $\Delta T$  of Case IV is 2.8 K (smaller than that of Case I) and the  $\sigma$  of Case IV is 1.57 (smaller than that of Case I), shows that the temperature uniformity is increased in Case IV. From Figure 7(a) and Figure 7(b), although the air flow resistance loss causes the downstream side temperature of the batteries along the flow direction to be still higher than the upstream temperature. The temperature difference among each battery group is reduced, and the thermal uniformity is improved, which is confirmed by smaller  $\Delta T$  and  $\sigma$ .

The comparison between the periodic airflow and similar methods is summarized in Table 3.

**Table 3.** The comparison between the periodic airflow and different air-cooling methods

Similar methods	Air supply parameter	Cells number	$T_{max}$ [K]	$\Delta T$ [K]	References
Unidirectional airflow	3 m/s	10	307.75	4.6	[30]
	2.5 m/s	8	319.95	5	[31]
Two-directional airflow	72 m <sup>3</sup> /h	12	306.25	4.5	[32]
Reciprocating airflow	5 m/s	12	315.45	9.8	[33]
Counterflow airflow	3 m/s	2	309.68	1.84	[34]
Periodic airflow	2 m/s	24	308	2.8	This paper

As shown in Table 3, compared with other cooling methods, the periodic airflow could maintain higher cooling efficiency at lower air supply velocity. Also, the battery pack could remain great uniformity with more cells by the periodic airflow method. Accordingly, the periodic airflow, with its good performance of low energy consumption and high uniformity, can better serve the energy storage batteries in the future.

## 5. CONCLUSIONS

In this paper, a simulation model is established for the container large-capacity energy system with lithium-ion rechargeable batteries, and the thermal characteristics of the system under conventional air-cooling conditions are analyzed. The influence of two airflow configurations on the thermal characteristics of the system is studied by numerical simulation, and the optimal design of the system is realized. On this basis, a new cooling method was proposed, and the relationship between thermal management and energy loss of the battery and different mass flow and temperature was studied. The main conclusions are as follows:

(1) The conventional directional air supply method has good heat dissipation performance only for the battery in the middle of the pack. But in fact, the temperature difference among each battery cells is large and the temperature uniformity is poor, which does not meet the working requirements.

(2) Improving the mass flow rate and decreasing the airflow temperature could both significantly increase the cooling performance of air convection compared to the basic case. But the temperature uniformity of batteries has no obvious improvement.

(3) The periodic airflow can decrease the highest temperature from 311 K to 308 K and decrease the temperature difference among each battery cells from 5.8 K to 2.8 K simply by changing the airflow

direction, which meets the working requirements and improves the thermal uniformity based on energy-saving.

#### ACKNOWLEDGEMENT

This research was supported by the Research Fund of Key Laboratory of Aircraft Environment Control and Life Support, MIIT, Nanjing University of Aeronautics and Astronautics (Grant No. KLAECLS-E-202001).

#### References

1. J. Luo, G.L. Tian, L.L. Zhang, Z.J. Li and J.Y. Wei, *Electrical Appliances and Energy Efficiency Management Technology*, 9(2019)49.
2. S.G. Yao, Y.H. Zhao, X.F. Sun, D.P. Ding and J. Cheng, *Int. J. Electrochem. Sci.*, 14(2019)2160.
3. Z.Q. Zhang, L. Jia, N. Zhao and L.X. Yang, *J. Therm. Sci.*, 20(2011)570.
4. H.J. Cao, S.H. Si, X.B. Xu, X.Y. Yang, J.F. Liu and S. Wu, *Int. J. Electrochem. Sci.*, 15(2020)4188.
5. Y.X. Qiao, X.Y. Wang, L.L. Yang, X.J. Wang, J. Chen, Z.B. Wang, H.L. Zhou, J.S. Zou and F.H. Wang, *J. Mater. Sci. Technol.*, 107(2022)197.
6. Y.B. Tang, X.W. Shen, Z.H. Liu, Y.X. Qiao, L.L. Yang, D.H. Lu, J.S. Zou and J. Xu, *Acta. Metall. Sin.*, 58(2022)324.
7. A. Boerger, J. Mertens and H. Wenzl, *J. Energy Storage*, 24(2019)100649.
8. Z.J. An, L. Jia, Y. Ding, C. Dang and X.J. Li, *J. Therm. Sci.*, 26(2017)391.
9. S. Wilke, B. Schweitzer, S. Khateeb and S. Al-Hallaj, *J. Power Sources*, 340(2017)51.
10. X.N. Feng, S.Q. Zheng, D.S. Ren, X.M. He, L. Wang, H. Cui, X. Liu, C.Y. Jin, F.S. Zhang, C.S. Xu, H.J. Hsu, S. Gao, T.Y. Chen, Y.L. Li, T.Z. Wang, H. Wang, M.G. Li and M.G. Ouyang, *Appl. Energy*, 246(2019)53.
11. A.A. Pesaran, *J. Power Sources*, 110(2002)377.
12. Q. Wang, B. Jiang, B. Li and Y.Y. Yan, *Renew. Sust. Energ. Rev.*, 64(2016)106.
13. Z.H. Rao and S.F. Wang, *Renew. Sust. Energ. Rev.*, 15(2011)4554.
14. R. Zhao, S.J. Zhang, J. Liu and J.J. Gu, *J. Power Sources*, 299(2015)557.
15. J.G. Wang, S. Lu, Y.Z. Wang, C.Y. Li and K.R. Wang, *J. Energy Storage*, 32(2020)101800.
16. F. He, H.T. Wang and L. Ma, *Int. J. Heat Mass Transf.*, 91(2015)630.
17. Z.Y. Fu, C.T. Lin and Q.S. Chen, *Journal of Highway and Transportation Research and Development*, 3(2005)119.
18. G. Zhang, L. Cao, S. Ge, C.Y. Wang, C.E. Shaffer and C.D. Rahn, *J. Electrochem. Soc.*, 161(2014)1499.
19. Z. Li, J.B. Zhang, B. Wu, J. Huang, Z.H. Nie, S. Ying, F.Q. An and N.N. Wu, *J. Power Sources*, 241(2013)536.
20. S. Panchal, I. Dincer, M. Agelin-Chaab, R. Fraser and M. Fowler, *Int. Commun. Heat Mass Transf.*, 71(2016)35.
21. S. Panchal, I. Dincer, M. Agelin-Chaab, R. Fraser and M. Fowler, *Int. J. Therm. Sci.*, 99(2016)204.
22. R. Mahamud and C. Park, *J. Power Sources*, 196(2011)5685.
23. G.D. Xia, L. Cao and G.L. Bi, *J. Power Sources*, 367(2017)90.
24. X.S. Wang, F. You, J.M. Zhang and Y.Z. Sun, *Energy Storage Science and Technology*, 5(2016)5770.
25. K.J. Yang, H.J. Pei, X.L. Zhu, Y.T. Zou, J.Y. Wang and H. Shi, *Energy Storage Science and Technology*, 9(2020)1858.
26. L.W. Fan, J.M. Khodadadi and A.A. Pesaran, *J. Power Sources*, 238(2013)301.

27. H. Shi, W.B. Xu, X.L. Zhu, J.Y. Wang, K.J. Yang, Y.T. Zou and Z.L. Chen, *Energy. Sci. Eng.*, 00(2022)1.
28. D. Bernardi, E. Pawlikowski and J. Newman, *J. Electrochem. Soc.*, 132(1985)5.
29. M.L. Li, M.Y. Zang, C.Y. Li and H.Y. Dai, *Battery Bimonthly*, 50(2020)266.
30. J.H. Xie, Z.J. Ge, M.Y. Zang and S.F. Wang, *Appl. Therm. Eng.*, 126(2017)583.
31. J.J. Zhang, X.L. Wu, K. Chen, D. Zhou and M.X. Song, *J. Power Sources*, 490 (2021) 229539.
32. K.H. Yu, X. Yang, Y.Z. Cheng and C.H. Li, *J. Power Sources*, 270 (2014) 193.
33. S.H. Hong, X.Q. Zhang, C. Kai and S.F. Wang, *Int. J. Heat Mass Transfer.*, 116 (2018) 1204.
34. X.C. Lin, K.K. Shao and C.H. Wang, *Int. J. Electrochem. Sci.*, 17(2022).

© 2022 The Authors. Published by ESG ([www.electrochemsci.org](http://www.electrochemsci.org)). This article is an open access article distributed under the terms and conditions of the Creative Commons Attribution license (<http://creativecommons.org/licenses/by/4.0/>).